Towards understanding and eliminating defects in additively manufactured CubeSat mirrors

Robert Snell, Carolyn Atkins, Hermine Schnetler, Younes Chahid, Mat Beardsley, Michael Harris, Chenxi Zhang, Richard Pears, Ben Thomas, Henry Saunders, Alexander Sloane, George Maddison, Iain Todd

Towards understanding and eliminating defects in additively manufactured CubeSat mirrors

Robert Snell[a], Carolyn Atkins[b], Hermine Schnetler[b], Younes Chahid[b], Mat Beardsley[c], Michael Harris[c], Chenxi Zhang[a], Richard Pears[a], Ben Thomas[a], Henry Saunders[a], Alexander Sloane[a], George Maddison[a], and Iain Todd[a]

[a]Department of Material Science and Engineering, University of Sheffield, UK
[b]UK Astronomy Technology Centre, Edinburgh, UK
[c]STFC Rutherford Appleton Lab, Didcot, UK

ABSTRACT

Fabricating mirrors using additive manufacturing (AM; 3D printing) is a promising yet under-researched production route. There are several issues that need to be better understood before AM can be fully adopted to fabricate mirror substrates. A significant obstacle to AM adoption is the presence of porosity and the influence that has on the resultant optical proprieties. Several batches of high-silicon aluminium (AlSi10Mg) samples were created to investigate the relationships laser parameters, laser paths and build orientations have with the porosity. The results showed that eliminating defects relies on a complex interaction of the process parameters and material properties, with the residual heating from the laser proving to be a significant factor. In addition, the use of a hot isostatic press is investigated and some full prototypes of the Cassegrain CubeSat were produced.

Keywords: Additive manufacturing, CubeSat, 3D printing, mirrors

1. INTRODUCTION

Additive manufacturing is a manufacturing technique that creates objects from powder rather than removing material from a solid block. The technique offers increased geometric freedom and the potential for lightweight designs that would be impossible using conventional machining methods. Many industries have invested heavily in AM, with aerospace and medical leading the way.[1] The most common AM technique is laser powder bed fusion, with layers of powder sequentially melted to form a solid object.

The use of AM among optical and astronomical engineering has increased in recent years but is still limited. A cluster of AM research came from an Horizon 2020 project. CubeSat mirrors,[2] deformable mirrors[3] and freeform optics[4] all featured as part of A2IM (Additive Astronomy Integrated-Component Manufacturing) within OPTICON (Optical Infrared Coordination Network for Astronomy).[5] This has led to offshoots from the A2IM team including Atkins et al.[6] as well as this research. Further examples have been used topology optimisation[7] and there has even been a recent review paper into the subject.[8]

In order to maximise the benefits of AM this project looks to fully integrate a Cassegrain mirror with the CubeSat mounting. The surface and structure will be made out of high-silicon aluminium (AlSi10Mg) and will not be coated with any nickel. The main limiting factor to this approach is the occurrence of porosity, which has a drastically adverse effect on the resultant optical surface.

This project aims to achieve an improved understanding of defect formation within AM and specifically within aluminium mirrors. On top of understanding the defects the work aims to control these defects, to ensure they are eliminated or at least minimised in the optical plane. Finally, this project will put the improved defect control in to action and work towards a CubeSat mirror which is lightweight and with an integrated mount.

Author contact details:
Robert Snell.: E-mail: r.m.snell@sheffield.ac.uk
Carolyn Atkins: E-mail: carolyn.atkins@stfc.ac.uk

2. ADDITIVE MANUFACTURING AND DEFECTS

While the promise and benefits of AM are clear there are still several obstacles that currently limit the adoption of AM. Defects, in their various guises, are a prominent part of these limitations. They weaken mechanical performance, reduce optical properties and make parts less predictable. The formation of defects depends on many factors. Most defects are related to the local thermal conditions and have a strong dependency on the processing conditions and the local laser-material interactions. Defects can depend on many other factors though; material composition, powder morphology and part geometry all play important roles in defect formation.[9]

The two most common forms of defects are pores and cracks. Pores are generally spherical voids within the material that form in a few different ways. Cracks also form in a few distinct ways, with the specifics usually depending on the material. Crack formation is heavily dependent on the material composition. Some extremely crack prone alloys can belong in the same family of alloys as alloys that are essentially crack-free (e.g. nickel superalloys).[10] There are many other material defects that may occur, depending on the composition, fluid dynamics and phase diagram of the alloy. As with casting, rolling or any other metallurgical process, the challenges are often material specific.

One final source of errors are surface defects. The surface roughness of AM materials is generally worse than cast or machined material. Surfaces can be especially problematic if they have sagging material from overhanging material.[11] Angled material is also subject to the stepping effect where non-vertical surfaces are limited in resolution by the layer thickness. Poor surface finishes, however, are not a major factor for optics applications. Any surface, AM or otherwise, would almost certainly require either polishing or turning. The underlying defects, in particular pores, are much more important for AM mirrors than the surface roughness.

2.1 Pores

There are three main types of pores in AM. These are lack of fusion (LoF), keyholes (KH) and gas entrapped bubble (GB). While these defects are all labelled as porosity they are distinct. The mechanisms by which they form are different, and the conventional classifications in terms size, form and frequency are also distinct, often though the exact criteria for the geometry of the defects can overlap.[9,12]

2.1.1 Lack of fusion

LoF pores are formed when the laser in the AM machine fails to melt all of the material it is required to in a layer. These generally occur when the process conditions are too cold, which might happen when the laser is too low in power or if the spacing between laser paths (hatch distance) is too large. LoF pores are generally large (up to 100 μm), have a low sphericity (irregular) and are elongated in the x-y plane (flattened in the build direction).[9,12]

2.1.2 Keyholes

KH pores are the contrast to LoF and form when the process conditions are too hot. The phenomena occurs when the laser melts too many layers down and leaves a void at the bottom of the deep melt pool. The occurance of KHs is also well documented in beam welding processes. The defects are often round and reasonably spherical, usually slightly elongated in the build direction.[9,12]

2.1.3 Gas entrapped bubbles

GB pores are usually the smallest pores (sub 10 μm) and are highly spherical. A common origin for these pores is porosity in the metal powder prior to melting. These pre-existing pores are reduced during the melting process but not fully eliminated. The prevalence of these defects depends on the atomisation method used creating the powder as well as the overall quality of the powder.[9,12]

There are other origin routes for GB pores. The melting process often involves the rapid melting of material and a turbulent meltpool. The turbulence as well as the phase changes within material can cast gas bubbles out into the material that are trapped in the solidifying the material. For many AM users GB pores are seen as the least consequential type of porosity and also the most difficult to avoid. The pores, given their small size, are often ignored and are the least likely to have an influence on many mechanical properties. This is an important distinction between most AM users and those wishing to use AM for mirrors and optics. Micron-scale pores are

of significance for mirror surfaces and do need to be considered when designing and processing an AM mirror surface.

3. LASER PARAMETER OPTIMISATION

3.1 Energy density equation

Calculating the optimal laser parameters for AM is not a trivial process. Process conditions need to be hot enough to fully melt the powder layer while avoiding the defects that occur with too high a temperature and boiling metal. The conditions also need to avoid macro-scale problem such as swelling. A useful estimation for calculating laser parameters is the energy density equation. This equation approximates the inputted laser energy divided by the volume of a powder layer. The energy density E is calculated using

$$E = \frac{P}{vht} \tag{1}$$

where P is the laser power, v is the laser speed, h is the hatch distance and t is the layer thickness. The optimal energy density for a material will depend on the thermal properties, the absorption of the laser energy and the specification of the powder.

A simplified version of the energy density equation uses the P and v terms to define linear energy density

$$E_{lin} = \frac{P}{v} \tag{2}$$

which is used define the laser interaction on a line by line basis. The equation also indicates how the same energy density can be achieved using many different laser power and speed combinations. A high power and high velocity laser can have the same energy density as a low power and low velocity laser, along with every increment in between.

The non-unique solutions on offer in the energy density equation also represent the limitations of the equation. Eventually the high power will become too high, causing boiling, and the low power too low, never melting the material. This will be true even if commensurate changes are made to the laser speed.

The limitations of the energy density equation are especially apparent with highly conductive materials, including the AlSi10Mg used in this research. The high conductivity means that for low or medium laser powers the result is a large warm volume of material rather than the desired smaller, hotter and molten region. Identical energy density values produce significantly different densities in these highly conductive materials. This result was documented by Prashanth et al.[13] and was further investigated as part of this research.

3.2 Design of experiments

As shown in equation 1 there are many parameters that can be varied when controlling the laser. All of the laser terms can be easily edited within the same build, i.e. building separate parts with different parameters at the same time. The only term that cannot be easily varied is the thickness of the powder layer. Variable layer thickness is possible using a very thin layer of powder and only melting parts when the correct number of layers have been dosed. The added time and difficulty means that this is not typically included as part of laser parameter optimisation. The powder layer depth used for the laser DoE was 30 μm and 50 μm for all other experiments in this report.

Even more terms can be varied that are not stated in the equation 1. Most AM machines have the function to adjust the shape and size of the laser beam. The laser focus can move the focal plane of the laser above or below or the build surface. This in turn alters the size of the beam, the power density and the shape (in this work the beam is Gaussian). The shape of the laser can also have a significant influence on the resultant thermal response in the material.

To navigate these many variables it is routine for some sort of design of experiments (DoEs) to be carried out to investigate these parameters. Often this means building several small cubes using different laser parameters,

followed by a rudimentary analysis of the material. This is an imperfect process, with slow steps and limitations on the insight that can be drawn, but it is often the easiest first step when working with a new alloy.

This process has been accelerated by building the samples (4 mm length cubes) onto cylinders (31.5 mm diameter) with walls. This configuration, as shown in Fig. 1, allows for the samples to be snapped off the base plate and to be polished without the need for cutting or sample mounting. This allows for 136 samples to be processed in hours rather than weeks.

Figure 1. A build plate with 136 AlSi10Mg cubes (length 4 mm) built on cylinders that are 31.5 mm diameters, to allow easy polishing.

The samples were built using AlSi10Mg powder (15 - 60 μm) supplied by Carpenter Additive. The samples were built using an Aconity Lab on an aluminium base plate in an argon atmosphere. The aluminium powder, aluminium base plate and the Aconity Lab system are used in every experiment in this research. The hatches were orientated to be aligned with the cube and with 90° rotations between each layer (i.e. North-South hatches followed by East-West hatches). This hatch pattern was chosen to reduce the effect of geometry and avoid having an overheating final corner on each layer.

Initially 136 samples were trialled with samples that were largely porous, due to too low energy densities and too high hatch spacings . An additional 136 samples were trialled with the intention of achieving KH pores and much tighter hatch spacings. Across the 272 samples the parameters were varied to find the not just optimal parameters but the extent to which the parameters could be pushed for each variable. The laser parameters used are summarised in Table 1.

Table 1. The laser parameters for DoE with AlSi10Mg

	First 136 samples	Second 136 samples
Laser power (W)	180 - 390	350 - 390
Laser speed (m/s)	0.50 - 1.75	0.9 - 3.0
Hatch distance (μm)	50 - 175	40 - 110
Energy density (J/mm^3)	42.7 - 104.0	60.9 - 156.7

The results of the DoE highlighted the limitations of the energy density estimations for aluminium. There were numerous examples of samples with similar energy densities having significantly different material outcomes. This was confirmed with findings by Prashanth et al.[13] The results showed that having a high laser power was critical to the success of the process, although this still needed to be matched with a suitable speed and hatch spacing. Some example cubes are shown in Fig. 2.
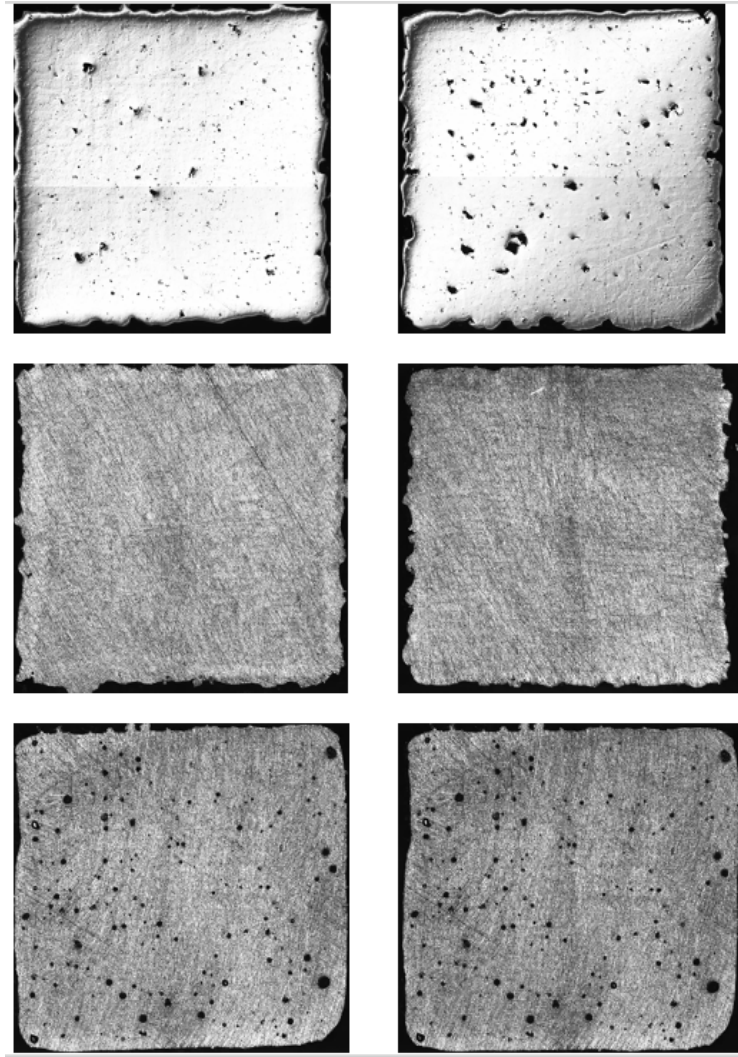

Figure 2. Example cubes from the DoE showing LoF (top), low porosity (middle) and KH (bottom).

There are were no distinct patterns when plotting material response (either density or pore type) against laser parameters, energy densities or any other derived equation using the laser parameters. The lack of a clear trend using just laser parameters is not unexpected. The unseen relationship as part of the energy density equation is that the energy density correlates with the size and the dynamics of the melt pool. In aluminium, with high values of conductivity, latent heats and reflectivity, this correlation breaks down and becomes difficult to predict.

This difficulty in applying the energy density equation is not always apparent, some materials have clear relationships and allow discrete regions of material outcome (i.e. KH domain, LoF domain, optimal domain, etc.) to be plotted in the parameter space.[14] Often research that attempt to work across multiple materials will segment models into separate parts for conductive (aluminium and copper alloys) and non-conductive materials (nickels and steels).

4. LASER PATH OPTIMISATION

One aspect not examined in the DoE is the path of the laser beam where the only change to the laser path is the variation of the hatch distance. The hatches are aligned so that the laser is parallel with the cube edges and the angle of the hatches between layers is 90°, for all samples and no other alterations are made. Rotating hatches are used in almost all AM settings. It allows for a more uniform application of the laser and prevents too hot or too cold regions developing. To further limit temperature variation some manufacturers use hatch angles that are not factors of 360 (e.g. 66° or 70°), this means the same hatch angle does not occur for many layers.

To investigate the affect of laser path a series of samples were built using different laser patterns as well as a few different laser parameters. The control sample used the same 90° rotating hatch used in the DoE experiments from earlier. Several samples used contours which feature melting around the perimeter of each layer while filling in the middle with hatches. For the samples that had multiple contours the contours were offset by the same distance as the hatch distance. An illustration of a contour laser path as well as an explanation of the hatch angle notation are shown in Fig. 3.
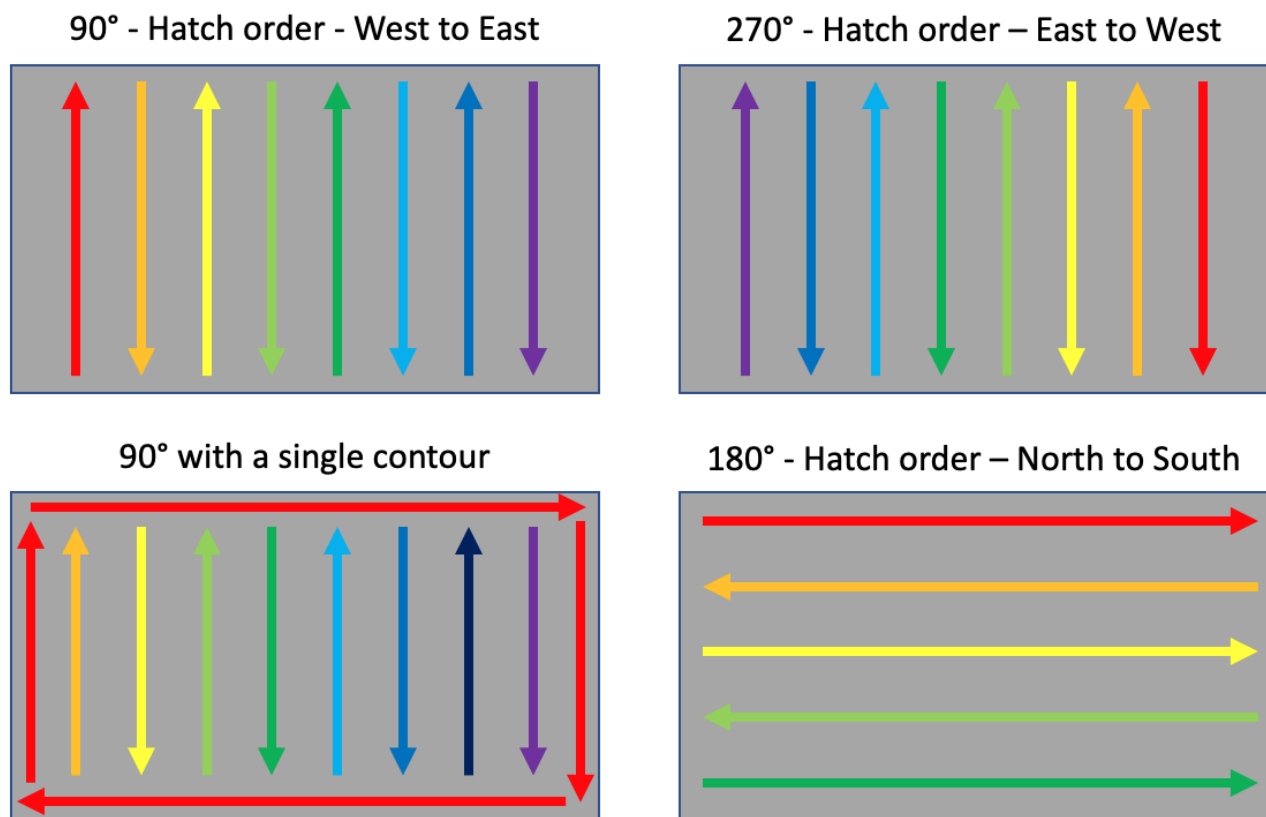

Figure 3. Some examples of the hatch order notation. The order of hatches goes from red through to purple. In the top left the hatches go from West to East, and so are noted with a 90° hatch angle. The laser melts in alternating North and South motions. The bottom left shows a contour pass. This involves a laser pass around the perimeter of the layer before melting the middle with a standard hatch pattern.

Non-standard angle changes were also employed, meaning that some samples were built with hatches only in certain directions. The laser path details are summarised in Table 2. The control laser parameters were 390 W, 1.1 m/s, 150 microns and focus offset of 1 mm. The 1 mm focus offset produces a slightly wider laser beam than a 0 mm focus, this was selected to match the standard aluminium parameters supplied with the AM machine. The layer depth was 50 μm.

Table 2. The laser parameters and patterns to investigate the laser path. Where no laser parameters or laser path are quoted the parameters and paths used in the control were duplicated.

Sample number	Laser parameters	Laser path
1	Control	0° start, 90° rotation
2		45° start, 90° rotation
3		66° start, 90° rotation
4		1 contour (contour last)
5		5 contours (contour last)
6		10 contours (contour last)
7		1 contour (contour first)
8		5 contours (contour first)
9		10 contours (contour first)
10		90° start, 180° rotation
11		0° start, 180° rotation
12		0° start, 0° rotation
13		90° start, 0° rotation
14	Power - 375 W Speed = 1.5 m/s	
15	Power - 390 W Speed = 1.0 m/s	

The geometry of the samples was designed to be similar to mirrors while making the processing as easy as possible. Cylinders with diameter 31 mm and depth 12 mm were built vertically (i.e. circle face perpendicular to the build direction). The diameter was selected to allow easy polishing through the standard microscopy sample processing. The bottom of the cylinder was replaced with small, inverted, truncated pyramids that could be easily snapped from the base plate. The samples are shown in Fig. 4.
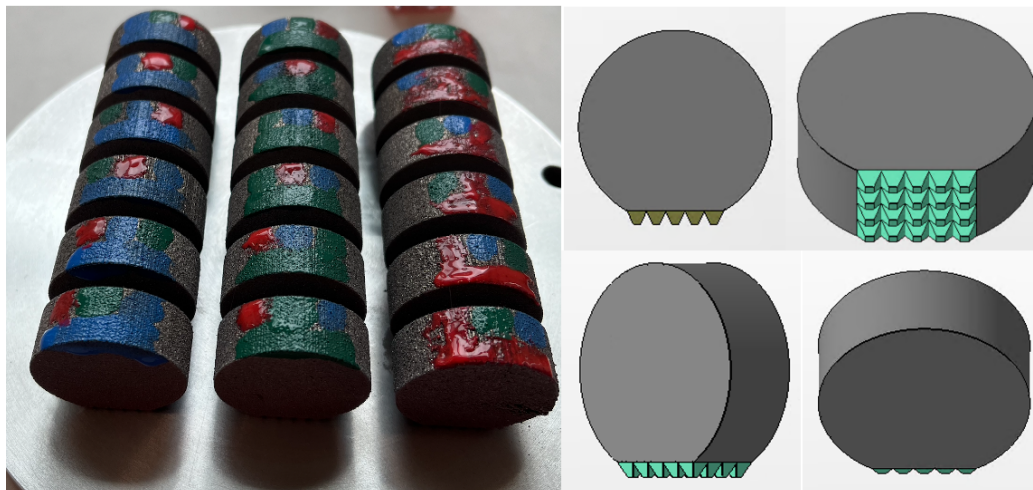

Figure 4. A photo and build image of the laser path samples.

The samples were snapped off the base plate manually and ground using automatic and manual polishing to a 2500 grit finish (approximately 8 μm finish). While this surface finish is much worse than the typical mirror quality required of these components, it is more than good enough for analysis of the defects and porosity.

The samples with fully rotating hatches (1, 2 and 3) all showed LoF defects. The middle sections of the contour samples showed similar levels of defects. A full investigation of the the contour samples was not possible as the polishing process ground through even the 10 contour samples. The edges of the contours were evident though, and left a very porous region between the hatch and contour interface.

Of particular interest were samples with restricted rotations. Samples 10 and 13, with hatches perpendicular to the mirror surface, showed no LoF porosity and much higher density values. Samples 11 and 12, with hatches parallel to the mirror surface, showed LoF defects similar to those seen in the fully rotating hatches. Some of the mirror surfaces are shown in Fig. 5.
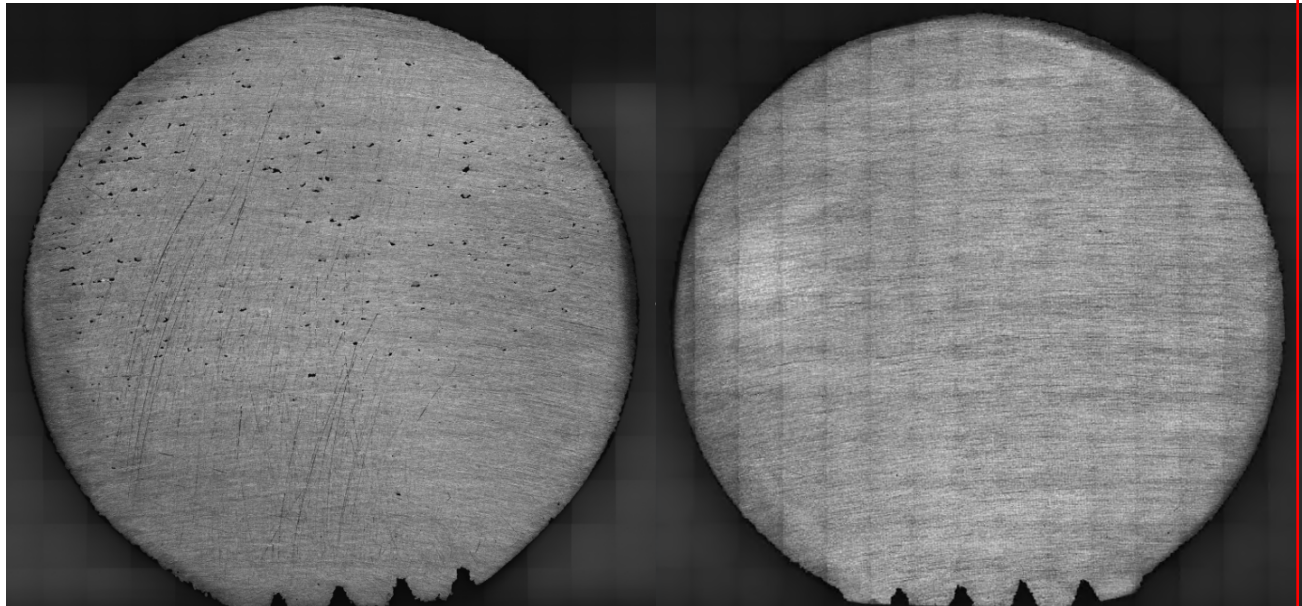

Figure 5. Images of the laser path optimisation samples. Sample 11 on the left shows LoF while sample 13 on the right does not. Formal density values are yet to be measured.

One theory that was investigated was based on work by Tammas-Williams et al.[15] The theory was that the end of the hatches leave a local area of high porosity. This would mean there is a thin region of porous material near the outer surface (within 0.5 mm). Past work in AM mirrors has found this layer of defects as material has been removed.

This effect of hatch-end porosity would have been evident in the samples with limited hatch rotations. Samples 10 and 13 would leave defects all along the mirror surface, while samples 11 and 12 would leave defects at the edge of the mirror surface. This effect was not observed. The likely explanation is that so much material was removed that it would have removed any of the expected porosity patterns.

The main difference in porosity was the opposite of the expected, with samples 10 and 13 giving excellent surfaces with close to no porosity. The explanation for this is likely due to the laser return time, explained in more detail in section 8.

5. PARAMETER INFLUENCE ON MIRROR SURFACES

The cylinders used in laser path investigation were a convenient compromise between a realistic representation of a mirror and convenience in processing the samples. However, given the influence geometry has on the material, it is necessary to use samples that are more like the type of mirrors that would be used in CubeSats and in

service generally. It was also necessary to process these mirrors in the same way a full prototype mirror would be processed, rather than the microscopy-type processing used earlier.

A simple mirror geometry was designed in order to investigate the porosity distribution in larger objects. The mirrors were single point diamond turned (SPDT) to a fine finish in order to measure the resultant mirror surfaces. The mirror surfaces are 50 mm in diameter and 4 mm in height, with three tabs to aid the SPDT process. The dimensions of the samples mirrors are shown in Fig. 6.
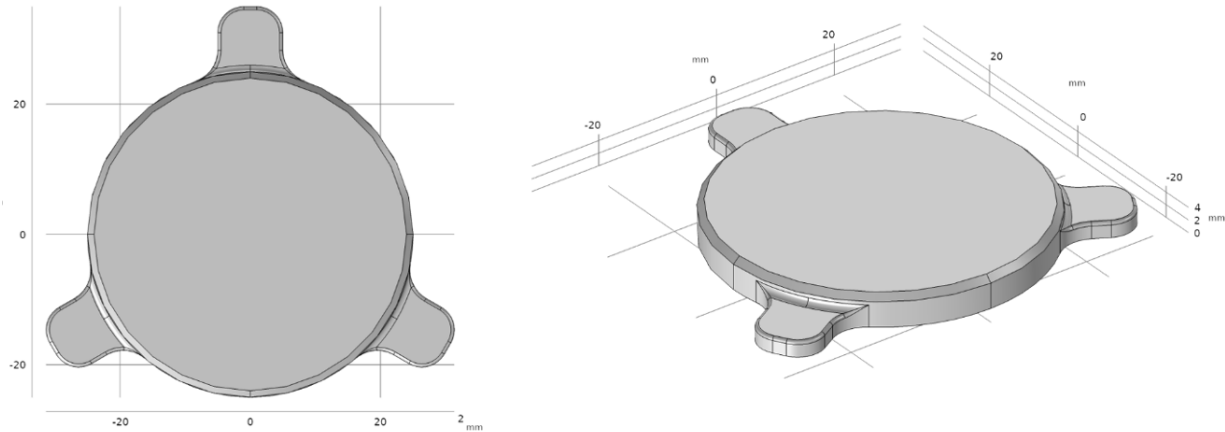

Figure 6. The dimensions of the simple mirrors that were produced and SPDT.

The initial trial involved three samples, all built horizontally (i.e. with the mirror face upwards), with varying laser parameters. The laser parameters are shown in Table. 3 along with the manufacturer listed parameters for AlSi10Mg. The powder and all other build details were the same as previous builds. Past experience had shown that the listed manufacturer parameters were susceptible to LoFs. As discussed earlier, while the situation may be quite complex it generally indicates the processing conditions are too cold.

Table 3. The laser parameters for the sample mirrors.

	Power (W)	Speed (mm/s)	Hatch (μm)
Aconity	375	1.5	150
Sample 1	375	1.6	150
Sample 2	375	1.4	150
Sample 3	375	1.2	150

All mirrors showed some defects, with some showing significant amounts of porosity and circular scratches (comet tails). The location and quantity of the defects provided some useful insight into the processing conditions. The lowest energy samples had the most defects and the highest energy samples had the fewest defects. It is a reasonable assumption that the higher energy density means a higher processing temperature, which means fewer LoF defects. Images of the mirror samples are shown in Fig. 7.

The location of the defects also reveals some useful information about the processing conditions. The defect density on all samples is higher in the middle of the samples. The second sample (with medium energy density) had porosity that was off to one direction. The location of the pores, like the laser path samples, is likely related to the laser return time (Section 8) as well as potentially the insulating effect of the loose powder. The loose (i.e. not melted) powder at the edge of a part offers better insulation than the solid (i.e. melted material) in the middle of a geometry. The net effect of this is the edges of the part get hotter and retain heat longer.
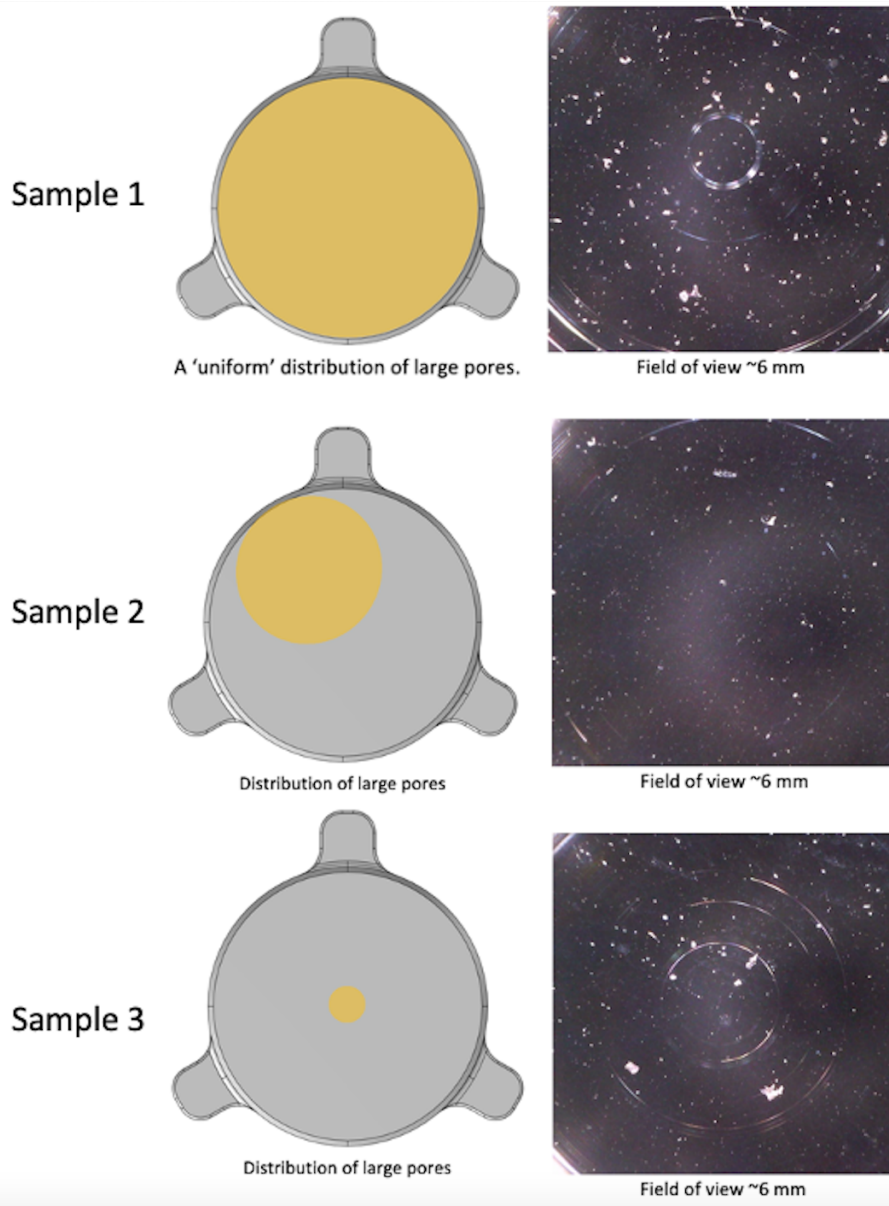
Figure 7. The horizontal mirrors built with highlighted regions indicating the areas with higher porosity and example defect regions for each sample.

6. BUILD ORIENTATION

A common practise in AM is to change the build orientation of a part. It may be easier to build a part on end, upside down or some other orientation. Often the deciding factor in selecting a build orientation is based on guidelines to minimise the chance of problems. Minimising negative space or reducing the amount of support material required are often the most important criteria. In mirrors though the quality of the mirror surface is of the upmost importance. If certain build angles can offer improved surface quality and defect-free material it is worth pursuing.

The same mirror geometry from before was built at 45° and vertically, as well as new horizontal samples. The laser parameters for all samples were changed to increase the processing temperature. The parameters used were 390 W, 1.1 m/s and 150 microns. The 45° mirror was built with the mirror surface on the upper side. Both

the vertical and 45° mirrors required supporting material to allow the building of the negative space (overhangs) under each mirror. The mirrors, with supporting material, are shown in Fig. 8.
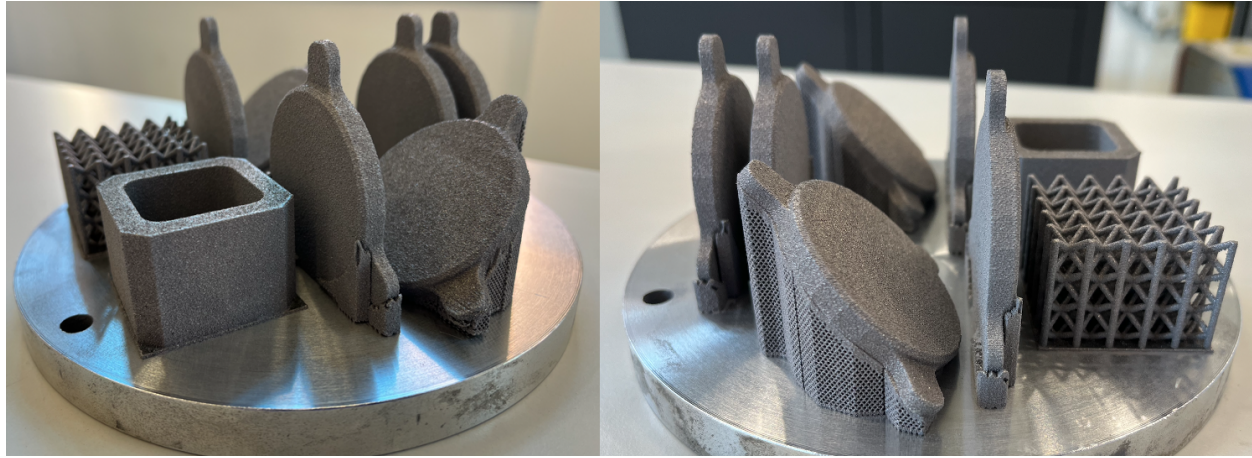

Figure 8. Photos of the mirrors built using different orientations. Also pictured are samples that were build at the same time but are not part of this research.

The results showed that the vertical mirrors produced the best surfaces. The 45° were the worst, although all samples had some amount of porosity and comet tails. The results again are likely due to the amount of melting the laser has to do on each layer. The vertical mirrors have thinner sections where higher temperatures are easier to achieve.

7. HOT ISOSTATIC PRESS

A common post-process technique for AM parts is to use a hot isostatic press (HIP). The process uses a high pressure and elevated temperature to remove internal defects from objects. The gas in internal defects is squeezed into the microstructure leaving either no defects or defects with greatly reduced volume.[16]

However, HIP is not a panacea for all material defects. If the defect is connected to the external of a part (e.g. a crack propagating through to the surface) then the defect cannot be closed using a HIP.[16] The closing of the defects can lead to part deformation, as the defects are closed the material contracts. Also if a part reaches an elevated temperature the defects can reform from the dissolved gas. Finally, the dimensions can also be a challenge with many HIPs unsuitable for the CubeSat mirrors used in this work.[16]

Despite the drawbacks, the benefits of defect removal are obvious for AM mirrors. Three 50 mm mirror samples were made in the three orientations as described in the previous section. These mirrors were all given a HIP treatment where they were heated to 500°C at a rate of 5 °C/min and pressure increased to 100MPa. The samples were held for 4 hours followed by natural cooling.

The HIPed samples showed improvements across all samples. Porosity and scratches were all reduced, with the vertical mirror samples having no detectable porosity under optical microscopy. It is not possible to declare the surface defect-free however, more thorough and precise measurements have to be carried out across the mirror surface. The HIPed surface did appear to have a slightly different color, specifically a milky colour, as seen in Fig. 9. The exact cause of this is unknown, although it is likely to be a physical change (e.g. very small scale roughness) rather than a chemical change (e.g. the absorbed gas changing the reflectivity).

Some deformation was evident where the mirrors warped across the surface. This was relatively minor however, and the polishing process was able to create a flat surface from the warped mirror surface. This deformation would be improved if the initial porosity was reduced. Using improved laser parameters and laser paths there would be less porosity and so less warping on future builds.
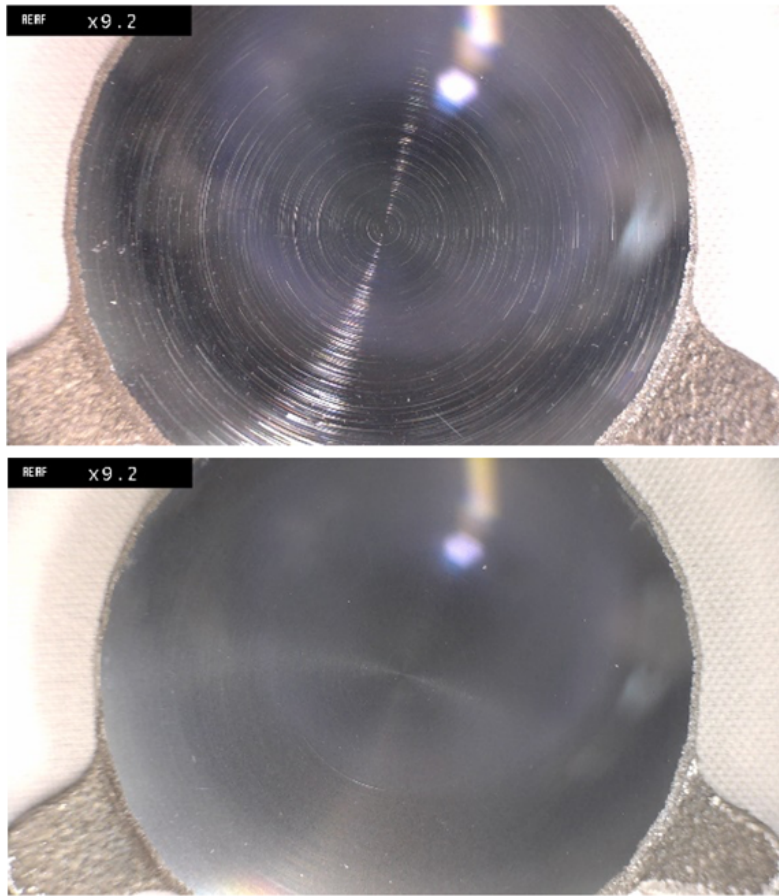
Figure 9. The non-HIP (top) and HIP (bottom) horizontal mirror samples.

8. LASER RETURN TIME

The concept of laser return time in AM is straight forward. For any given hatch the laser will not be encountering metal powder at room temperature. The heat from the previous laser hatch will have warmed the surrounding material and mean that the current hatch reaches a higher temperature. The laser return time is a measurement of how recent the laser was melting the previous hatch. Short hatches will have a short laser return time and result in the largest temperature increase. Longer hatches will have a longer wait between laser passes and so will be colder.

An example of the effect laser return time has is shown in the laser path samples. Samples 10 and 13 only have hatches in the short direction (12 mm) and so show no LoF pores. Samples 11 and 12 have hatches that go the full width of the samples (upto 31 mm) and so are much colder and result in LoF formation. The control samples and other fully rotating samples also contain layers with long hatches (although not every layer) but this still results in LoF.

The effect of short hatches and long hatches is negated at the top of the laser path samples. The cylinders are close to complete here and so the area melted is closer to a square than an elongated rectangle. The difference between 0° hatches and 90° hatches is therefore greatly reduced, which is evident in the lack of LoF pores at the top of these samples.

Laser return time only takes into account the time from the previous hatch. A more thorough way of measuring this effect though takes into account all previous hatches. As hatches occur longer ago in time and further away in distance then the influence of each hatch will diminish. The approximation using all hatches is

referred to as the local laser energy (LLE). An analysis was done on the hatches at 0° and 90° at several layer heights. An example set of results are shown in Fig. 10.
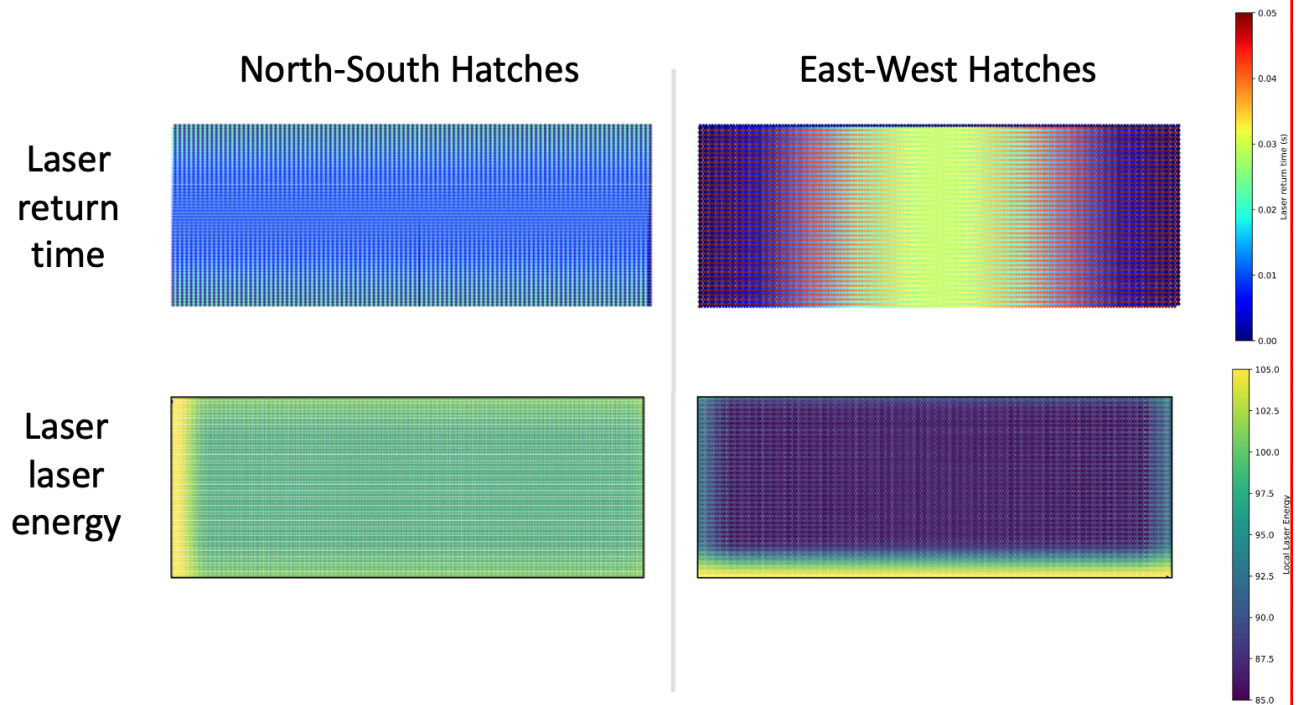

Figure 10. Diagrams showing the return times and LLE for the different hatch setups at the midpoint of the cylinder.

The patterns of the two laser return times have some similarities. The edges where the hatches end and start have alternating high and low values. The middle is more of a uniform value. The difference in the values though reveals the difference between the hatch orientations. The middle of East-West has a uniformly high laser return time.

The LLE analysis is generally more uniform throughout the layer than the laser return time. This is to be expected given the measurement is more of an average than just using the details of the previous hatch. The difference between the hatch angles is even more obvious, the East-West hatch has a very low value through the part where as the North-South has a much higher value.

9. DESIGN CONCEPTS

If mirror quality and porosity distribution were the only factors to consider then the work so far would point to a likely mirror design. A thin mirror, built vertically, would allow for consistent, high temperature processing conditions on every layer. However, it is necessary to consider the type of mirror that is desired and how easy it will to build in a vertical direction. A sandwich mirror has been the mirror of choice for this work from the start, with the middle of the sandwich being some sort of lattice designed to be as stiff as possible during the polishing or turning process.

This is the inevitable problem with building the mirrors vertically. The material required to support the mirror surface is perpendicular to the build direction, which is extremely problematic. The overhangs or negative space would cause build failures for most of the proposed lattice solutions for this work. Compromising the design to accommodate a vertical build would limit the benefits in terms of weight, print-through mitigation and the stiffness of the part.

9.1 Lattice concepts

The main concept behind these lattices builds on previous work by Snell et al.[2] and Atkins et al.[17] The unit cell in these designs is not a fixed shape. It it is design to tessellate and fit exactly within the area of the mirror. This avoids having unsupported material or weighty infills around the mirror circumference. The unit cell shape can be either be a triangle or curved quadrilateral.

The initial work used lattices that were essentially modified BCCz lattices. Due to problems with thermal stresses the designs were made more conservative in terms of weightsaving. Solid polyhedrons were introduced, either in the form of triangle-based or square-based pyramids. The most conservative design had a pyramid intersecting with an inverted pyramid, called the hourglass design. A later design replaced the lower pyramid with a lattice strut, referred to as the martini glass design. The hourglass design, using a quadrilateral based lattice, was successfully built in AlSi10Mg. The mirror can be seen in Fig. 11.
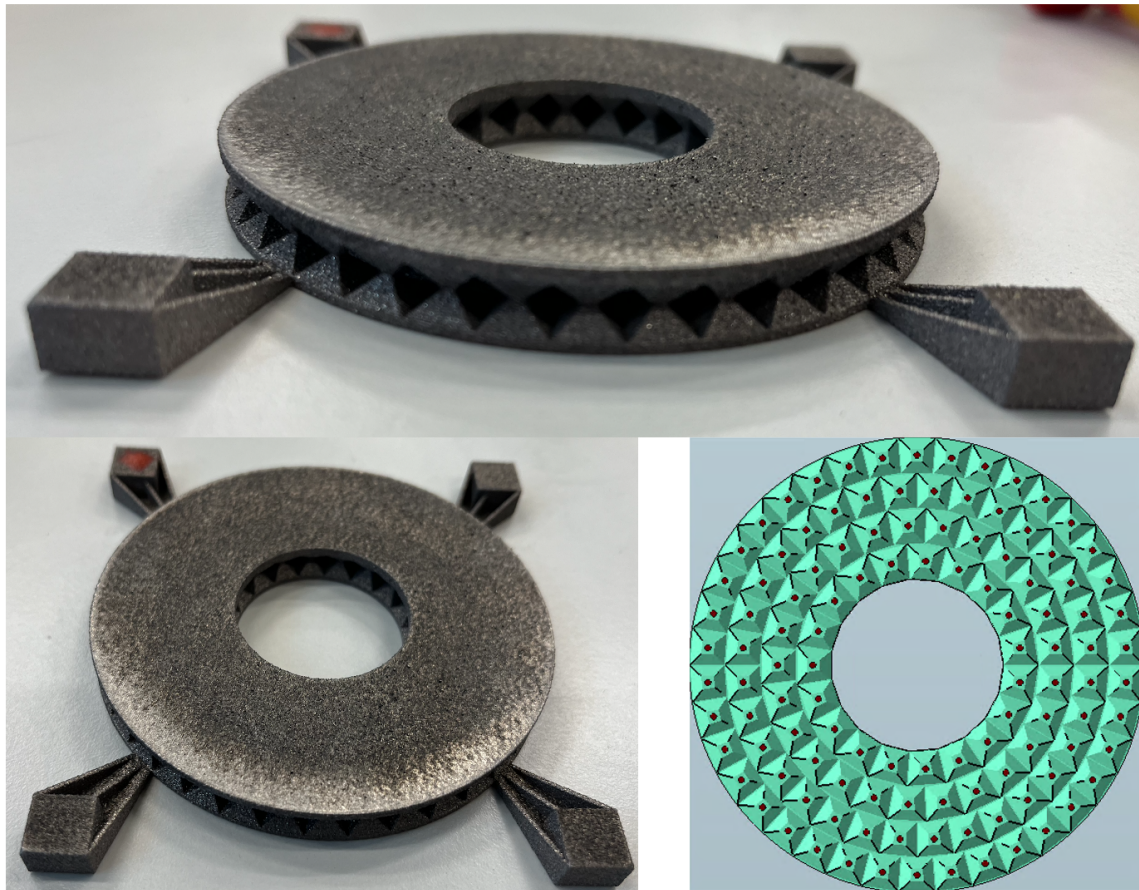

Figure 11.   Photos of the hourglass mirror and a cross-section of the unit cells.

An attempt was made to build the martini glass design using the same base and unit cell map. The build was unsuccessful, with thermal stress pulling the lattice apart. Changes in build technique have significantly improved the control of thermal stress, largely based on reducing the time between build layers. A heated bed could be a viable solution but a suitable machine with a large enough build plate was not available. Efforts are currently being made to better understand the thermal stress forces as well as alternative strategies for mitigating the effects. The results of the thermal stress are shown in Fig. 12.
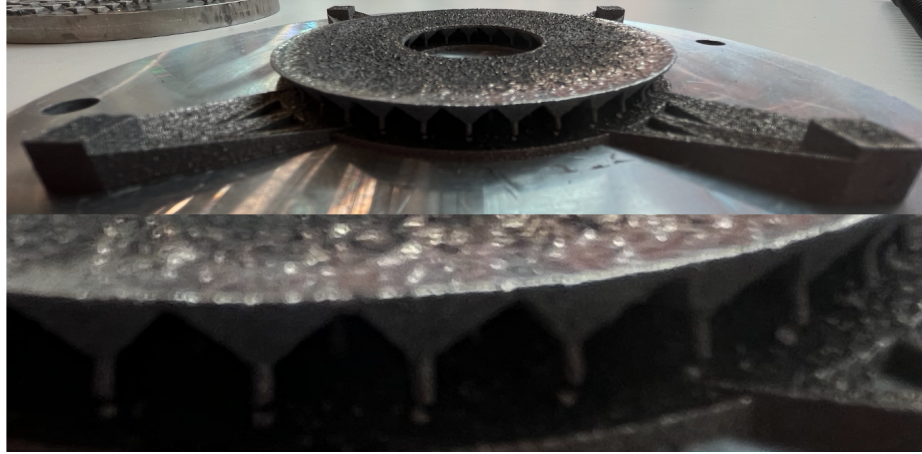
Figure 12. Photos of the martini glass mirror with a zoomed in view on failed lattice struts. The struts have disconnected with the base around the outer edge due to the thermal stresses during production.

10. SUMMARY AND FUTURE WORK

The results so far have revealed a great deal of useful data that have enhanced our understanding of defect formation and will allow for production of defect-free mirrors. More generally, it has also shown how interconnected all of these design considerations. The best laser parameters depend on the laser path, which in turn depends on the build orientation, which depends on the build design.

The work so far has largely been about understanding the standard way of doing things. While this is not comprehensive, there is enough knowledge now to attempt more unusual methods. Non-standard laser paths, sintering of the surrounding powder and variable laser parameters are all potential options.

Finally, the research has been mostly discrete. In order to better understand individual aspects of the process the other aspects have been set to a constant. The next stages of this research will bring the insight from the different aspects into a single plan for designing and building defect-free mirrors.

REFERENCES

[1] Gibson, I., "The changing face of additive manufacturing," *Journal of Manufacturing Technology Management* (2017).

[2] Snell, R., Atkins, C., Schnetler, H., Todd, I., Hernandez-Nava, E., Lyle, A. R., Maddison, G., Morris, K., Miller, C., Roulet, M., Hugot, E., Sangines, F. T., Vega-Moreno, A., van de Vorst, L. T. G. B., Dufils, J., Brouwers, L., Farkas, S., Mezo, G., Beardsley, M., and Harris, M., "An additive manufactured CubeSat mirror incorporating a novel circular lattice," in [*Advances in Optical and Mechanical Technologies for Telescopes and Instrumentation IV*], Navarro, R. and Geyl, R., eds., **11451**, 58 – 73, International Society for Optics and Photonics, SPIE (2020).

[3] Roulet, M., Atkins, C., Hugot, E., Snell, R., van de Vorst, B., Morris, K., Marcos, M., Todd, I., Miller, C., Dufils, J., Farkas, S., Mezo, G., Tenegi, F., Vega-Moreno, A., and Schnelter, H., "Use of 3D printing in astronomical mirror fabrication," in [*3D Printed Optics and Additive Photonic Manufacturing II*], Herkommer, A. M., von Freymann, G., and Flury, M., eds., **11349**, 33 – 44, International Society for Optics and Photonics, SPIE (2020).

[4] Farkas, S., Agocs, T., Atkins, C., Brouwers, L., Dufils, J., Joo, A., Mezo, G., Morris, K., Rodenhuis, M., Roulet, M., Schnetler, H., Snell, R., Tenegi-Sangines, F., Vega-Moreno, A., and van de Vorst, B., "Freeform active mirror designed for additive manufacturing," in [*Advances in Optical and Mechanical Technologies for Telescopes and Instrumentation IV*], Navarro, R. and Geyl, R., eds., **11451**, 526 – 534, International Society for Optics and Photonics, SPIE (2020).

[5] Schnetler, H., van de Vorst, B., Snell, R. M., Atkins, C., Miller, C., Morris, K., Farkas, S., Mezo, G., Roulet, M., Hugot, E., Moreno, A. V., Tenegi, F., and Dufils, J., "H2020 opticon WP5 overview: investigating the use of additive manufacturing AM) for the design and build of multifunctional integrated astronomical components," in [*Advances in Optical and Mechanical Technologies for Telescopes and Instrumentation IV*], Navarro, R. and Geyl, R., eds., **11451**, 357 – 377, International Society for Optics and Photonics, SPIE (2020).

[6] Atkins, C., Brzozowski, W., Dobson, N., Milanova, M., Todd, S., Pearson, D., Bourgenot, C., Brooks, D., Snell, R., Sun, W., Cooper, P., Alcock, S. G., and Nistea, I.-T., "Additively manufactured mirrors for CubeSats," in [*Astronomical Optics: Design, Manufacture, and Test of Space and Ground Systems II*], Hull, T. B., Kim, D. W., and Hallibert, P., eds., **11116**, 335 – 352, International Society for Optics and Photonics, SPIE (2019).

[7] Horvath, N. and Davies, M., "Advancing lightweight mirror design: a paradigm shift in mirror preforms by utilizing design for additive manufacturing," *Appl. Opt.* **60**, 681–696 (Jan 2021).

[8] Zhang, K., Qu, H., Guan, H., Zhang, J., Zhang, X., Xie, X., Yan, L., and Wang, C., "Design and fabrication technology of metal mirrors based on additive manufacturing: A review," *Applied Sciences* **11**(22) (2021).

[9] Kim, F. H., Kim, F. H., and Moylan, S. P., [*Literature review of metal additive manufacturing defects*], US Department of Commerce, National Institute of Standards and Technology . . . (2018).

[10] Sanchez-Mata, O., Wang, X., MuÃ±iz-Lerma, J. A., Attarian Shandiz, M., Gauvin, R., and Brochu, M., "Fabrication of crack-free nickel-based superalloy considered non-weldable during laser powder bed fusion," *Materials* **11**(8) (2018).

[11] Sanaei, N. and Fatemi, A., "Analysis of the effect of surface roughness on fatigue performance of powder bed fusion additive manufactured metals," *Theoretical and Applied Fracture Mechanics* **108**, 102638 (2020).

[12] Snell, R., Tammas-Williams, S., Chechik, L., Lyle, A., Hernandez-Nava, E., Boig, C., Panoutsos, G., and Todd, I., "Methods for rapid pore classification in metal additive manufacturing," *JOM* **72**(1), 101–109 (2020).

[13] Prashanth, K. G., Scudino, S., Maity, T., Das, J., and Eckert, J., "Is the energy density a reliable parameter for materials synthesis by selective laser melting?," *Materials Research Letters* **5**(6), 386–390 (2017).

[14] Johnson, L., Mahmoudi, M., Zhang, B., Seede, R., Huang, X., Maier, J. T., Maier, H. J., Karaman, I., Elwany, A., and ArrÃ³yave, R., "Assessing printability maps in additive manufacturing of metal alloys," *Acta Materialia* **176**, 199–210 (2019).

[15] Tammas-Williams, S., Zhao, H., LÃ©onard, F., Derguti, F., Todd, I., and Prangnell, P., "Xct analysis of the influence of melt strategies on defect population in ti6al4v components manufactured by selective electron beam melting," *Materials Characterization* **102**, 47–61 (2015).

[16] Tammas-Williams, S., Withers, P. J., Todd, I., and Prangnell, P. B., "The effectiveness of hot isostatic pressing for closing porosity in titanium parts manufactured by selective electron beam melting," *Metallurgical and materials transactions A* **47**(5), 1939–1946 (2016).

[17] Atkins, C., Brzozowski, W., Dobson, N., Milanova, M., Todd, S., Pearson, D., Bourgenot, C., Brooks, D., Snell, R., Sun, W., Cooper, P., Alcock, S. G., and Nistea, I.-T., "Lightweighting design optimisation for additively manufactured mirrors," in [*Astronomical Optics: Design, Manufacture, and Test of Space and Ground Systems II*], Hull, T. B., Kim, D. W., and Hallibert, P., eds., **11116**, 353 – 371, International Society for Optics and Photonics, SPIE (2019).